Extension of the mechanoresponsive luminescence shift via formation of a doped organic crystal

Ryohei Yoshida,[a] Takashi Tachikawa*[b,c] and Suguru Ito*[a,d]

[a] *Department of Chemistry and Life Science, Graduate School of Engineering Science, Yokohama National University*
79-5 Tokiwadai, Hodogaya-ku, Yokohama 240-8501, Japan
*E-mail: suguru-ito@ynu.ac.jp

[b] *Department of Chemistry, Graduate School of Science, Kobe University,*
1-1 Rokkodai-cho, Nada-ku, Kobe 657-8501, Japan

[c] *Molecular Photoscience Research Center, Kobe University,*
1-1 Rokkodai-cho, Nada-ku, Kobe 657-8501, Japan
*E-mail: tachikawa@port.kobe-u.ac.jp

[d] *PRESTO, Japan Science and Technology Agency (JST),*
4-1-8 Honcho, Kawaguchi, Saitama 332-0012, Japan

Table of contents

1. General

Fluorescence and UV-vis absorption spectra were measured on a JASCO FP-8300 fluorescence spectrometer. The solid-state absorption spectra were obtained by measuring diffuse reflectance spectra using an FPA-810 powder sample cell block, in which a sample diluted in $BaSO_4$ (10 wt%) was loaded. The absolute fluorescence quantum yields were determined using a 100 mm ϕ integrating sphere JASCO ILF-835. A miniature fiber-optic spectrometer (FLAME-S-XR1-ES, Ocean Optics) was used for the measurements of crystalline and ground bulk samples. PXRD measurements were performed on a Rigaku SmartLab system using CuKα radiation. DSC data were recorded on a Shimadzu DSC-60 plus instrument (heating rate: 10 °C min^{-1}). 4-(2-Thienyl)-2,1,3-benzothiadiazole (**1**)[1] and 4,7-di(2-thienyl)-2,1,3-benzothiadiazole (**2**)[2] were synthesized according to the literature procedures.

2. Preparation of doped mixed crystals

*Typical procedure for the preparation of doped mixed crystals **1•2** (250 ppm)*

A THF solution of **1** (1.0×10^{-1} M, 5.0 mL) was mixed with a dilute THF solution of **2** (5.0×10^{-3} M, 25 μL), and the solvent of the mixture was evaporated under reduced pressure. The residue was dissolved in hot cyclohexane (0.8 mL, 50 °C), and the solution was cooled to room temperature to give doped mixed crystals **1•2**.

The ratio of **2** to **1** in the doped crystals **1•2** (250 ppm) was determined by HPLC analysis (Chiralcel OD-H; 254 nm UV detector; eluent, hexane/*i*-PrOH = 9:1; flow rate, 0.5 mL/min; *t*, 10.4 min for **1**, 15.4 min for **2**). Although the amount of **2** included in **1•2** varied from crystal to crystal, it was typically in the range of $(3.7\pm1.6) \times 10^2$ ppm (Table S1).

Table S1. The ratio of **2** in the doped crystals

Entry	Ratio of **2** (ppm)	Entry	Ratio of **2** (ppm)
1	234	5	138
2	621	6	310
3	346	7	390
4	211	8	671

3. Single-crystal X-ray structure of 1

The single-crystal X-ray structure of **1** (CCDC2111903)[1] supports the probability that the molecule of **2** is included in the crystal structure (Fig. S1). Focusing on a pair of **1** shown in orange, other pairs are stacked above and below the orange pair (Fig. S1a and b). Moreover, the front and back sides as well as left and right sides of the orange pair are surrounded by other vertically oriented pairs (Fig. S1c and d). Although the molecular size of **2** is larger than that of **1**, the inclusion of **2** in the crystal structure should be achieved by replacing the pair of **1** with a single molecule of **2**.

The density functional theory (DFT) calculations of stacked **1•2** were performed using the Gaussian 16 program.[3] The stacked **1•2** was generated by attaching 2-thienyl group to the one molecule of the stacked two molecules of **1** obtained from the single-crystal X-ray diffraction analysis. The calculated HOMO and LUMO of the stacked **1•2** at the CAM-B3LYP/6-31G(d) level of theory are shown in Fig. S1e. BSSE was taken into account using the counterpoise correction.[4] Both HOMO and LUMO of the stacked **1•2** are mainly located on **2**. Accordingly, the new absorption band of crystalline **1•2** (Fig. 2c) would be attributed to the HOMO-LUMO transition of **2** rather than charge-transfer transitions from **1** to **2**.

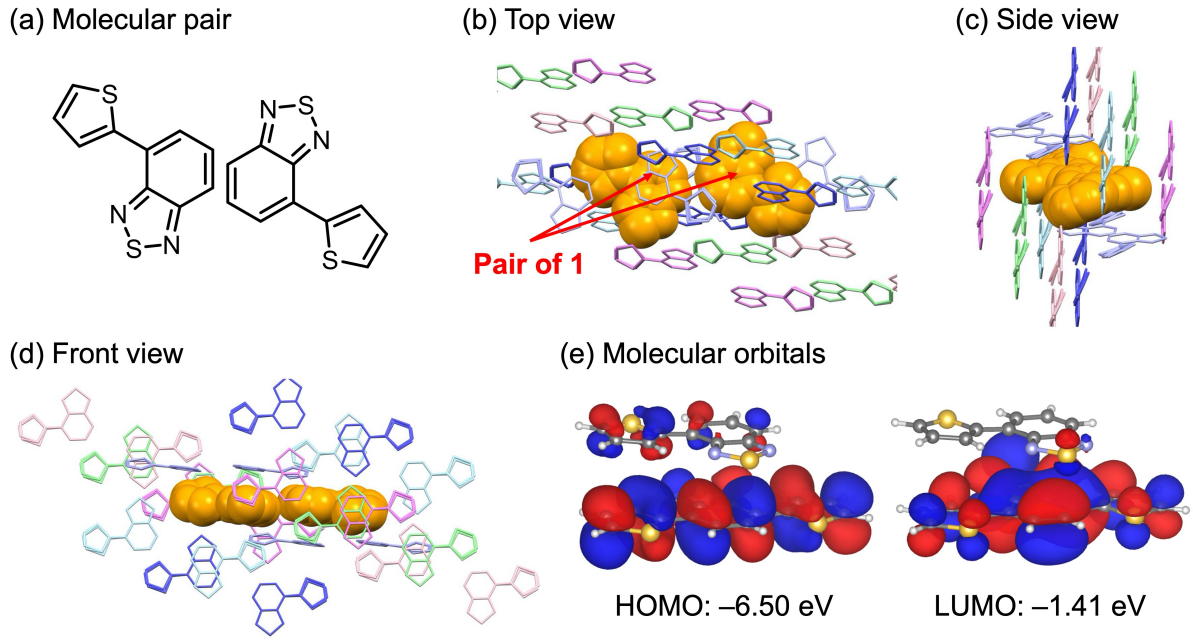

Fig. S1 (a) Pair of **1**. (b) Top, (c) front, and (d) side view of the crystal structure of **1**. The orange-colored space-filling model represents the pair of **1**. All hydrogen atoms are omitted for clarity. (e) HOMO and LUMO of **1•2** calculated at the CAM-B3LYP/6-31G(d) level. The structures are drawn by VESTA.[5]

4. Supplementary spectra for the emission switching

Fluorescence spectra of **1** and **2** showed hypsochromic shifts in maximum emission wavelength from 502 nm to 492 nm (Fig. S2a) and from 617 nm to 590 nm (Fig. S2b), respectively. The maximum emission wavelength of crystalline **1•2** (1000 ppm) was shifted in the hypsochromic direction from 575 nm to 561 nm upon grinding ($\Delta\lambda_{em}$ = 14 nm), and the intensity of the short-wavelength region slightly increased in the emission spectra of ground **1•2** (1000 ppm) (Fig. S2c).

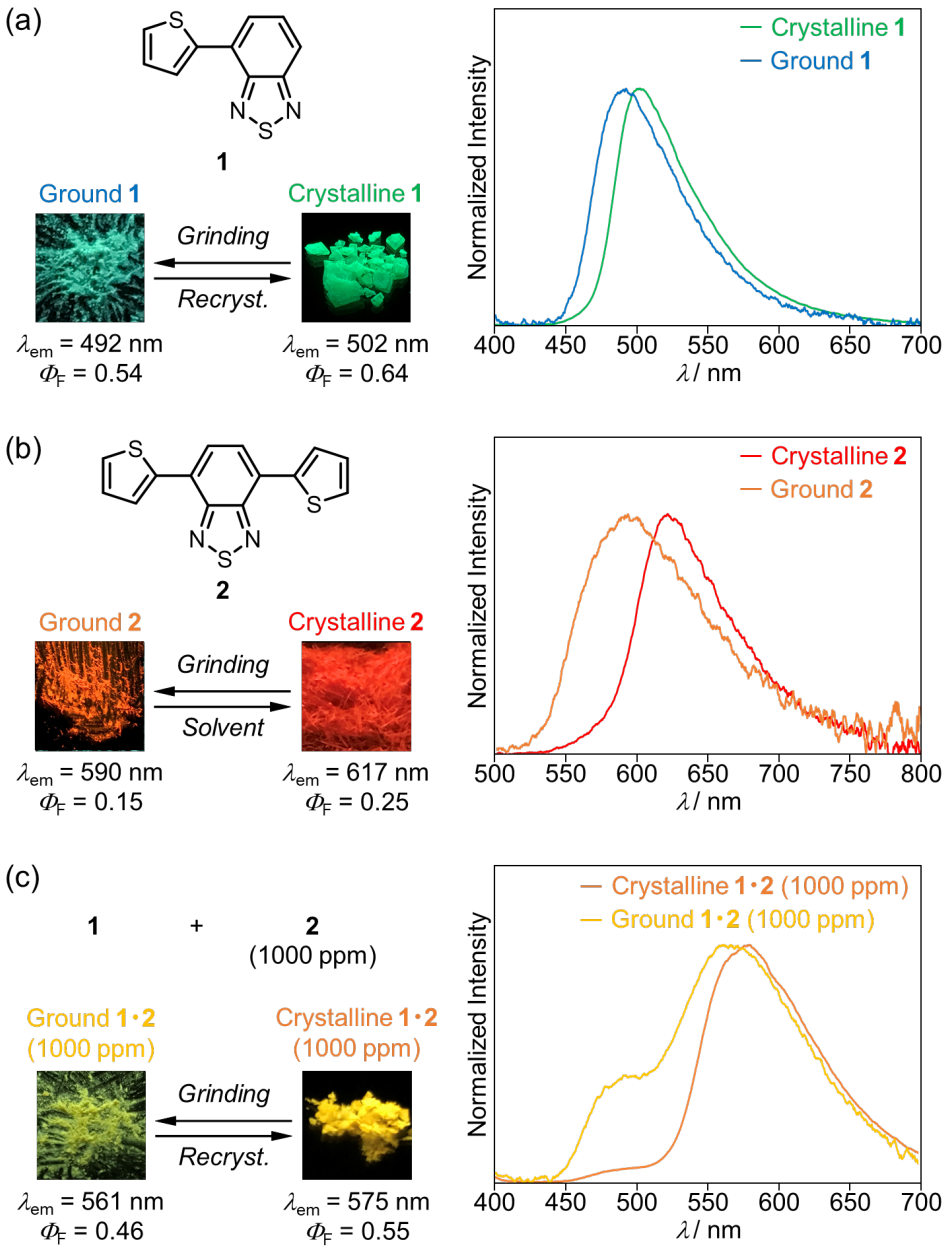

Fig. S2 Photographs and fluorescence spectra for the emission switching of (a) **1**, (b) **2**, and (c) **1•2** (1000 ppm) (λ_{ex} = 365 nm).

5. Supplementary absorption and excitation spectra

The solid-state absorption spectra were obtained by measuring diffuse reflectance spectra of samples diluted in $BaSO_4$ (10 wt%). The observed reflectance spectra (%R = $I/I_0 \times 100$) were converted to absorbance [Abs = $\log(I_0/I)$]. Since crystalline samples change their photophysical properties upon grinding, small crystalline samples (each ca. 1.0 mm length) were carefully mixed with $BaSO_4$ on a mortar using a pestle with a mixing pressure not exceeding 5.0 N cm^{-2} (Table S2). Ground samples for absorbance measurements were prepared by grinding the mixture of crystalline samples with $BaSO_4$ on a mortar using a pestle with a grinding pressure above 70 N cm^{-2}.

The absorption spectrum of crystalline **1** was almost identical to that of ground **1** (Fig. S3a). The absorption band of crystalline **1•2** (1000 ppm) at around 500 nm was significantly reduced after grinding (Fig. S3b). The absorption spectra of crystalline **1**, crystalline **2**, and crystalline **1•2** (250 ppm) are shown in Fig. S3c for comparison. Since the crystalline samples are relatively large and heterogeneous in particle size, the relative concentrations of **1** and **2** in the doped crystals are not reflected in the absorbance spectra even after the Kubelka-Munk treatment (Fig. S3d).

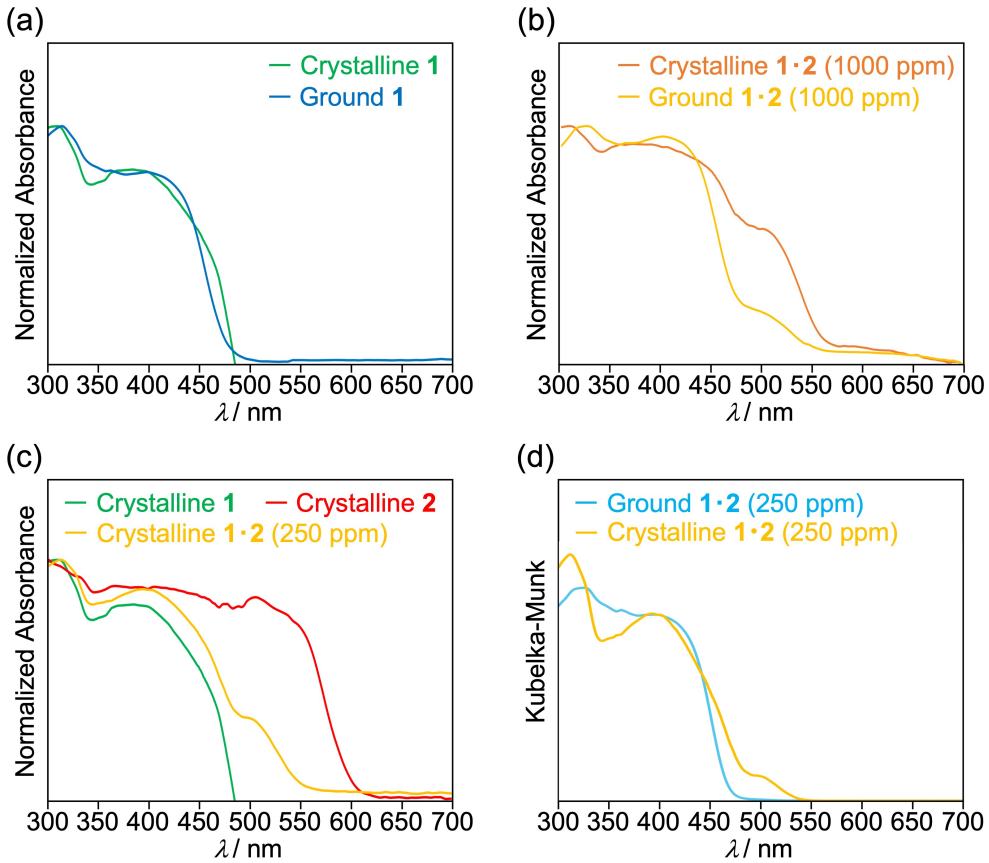

Fig. S3 Absorption spectra for emission switching of (a) **1** and (b) **1•2** (1000 ppm). (c) Absorption spectra of crystalline **1**, **2**, and **1•2** (250 ppm). (d) Absorption spectra of crystalline and ground **1•2** (250 ppm) after the Kubelka-Munk treatment.

The excitation band of crystalline **1•2** (250 ppm) at around 500 nm was significantly reduced after grinding (Fig. S4).

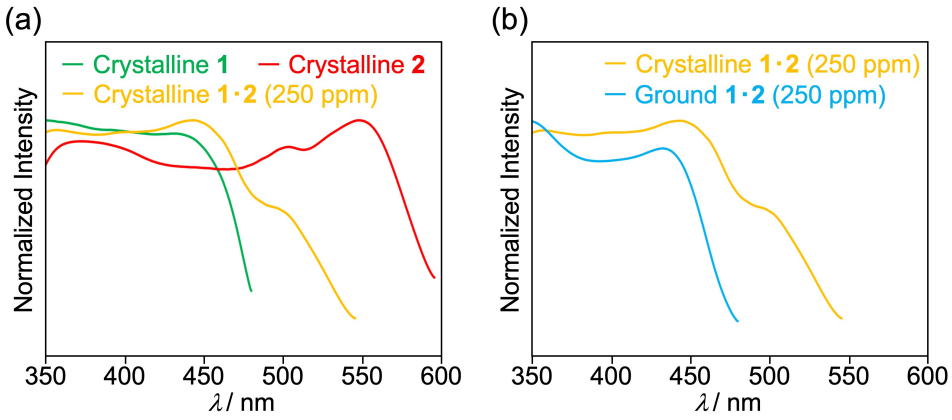

Fig. S4 Excitation spectra of (a) crystalline **1**, **2**, and **1•2** (250 ppm) and (b) crystalline and ground **1•2** (250 ppm) observed at their maximum emission wavelengths.

6. Supplementary spectra to compare ground 1•2 and ground 1

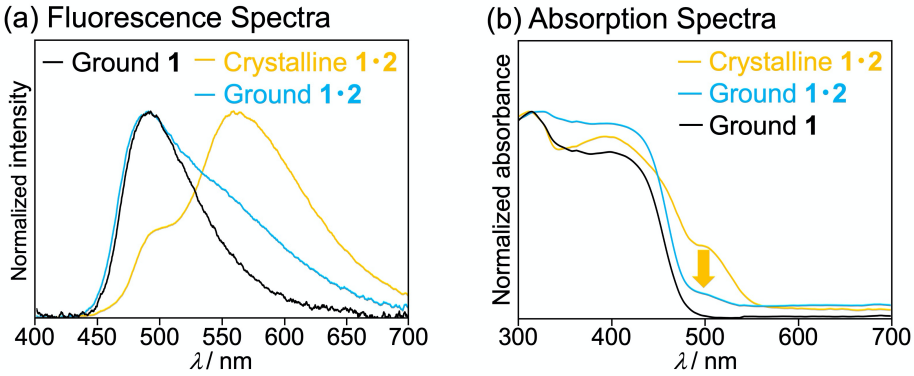

Fig. S5 (a) Fluorescence spectra of crystalline **1•2**, ground **1•2**, and ground **1** (λ_{ex} = 365 nm). (c) Absorption spectra of crystalline **1•2**, ground **1•2**, and ground **1**.

7. PXRD analyses

PXRD patterns showed that the intensity of diffraction peaks in crystalline samples decreased after grinding (Fig. S6). The hypsochromic shift of the wavelength maxima in response to mechanical stimuli should result from the partial destruction of the molecular arrangements.

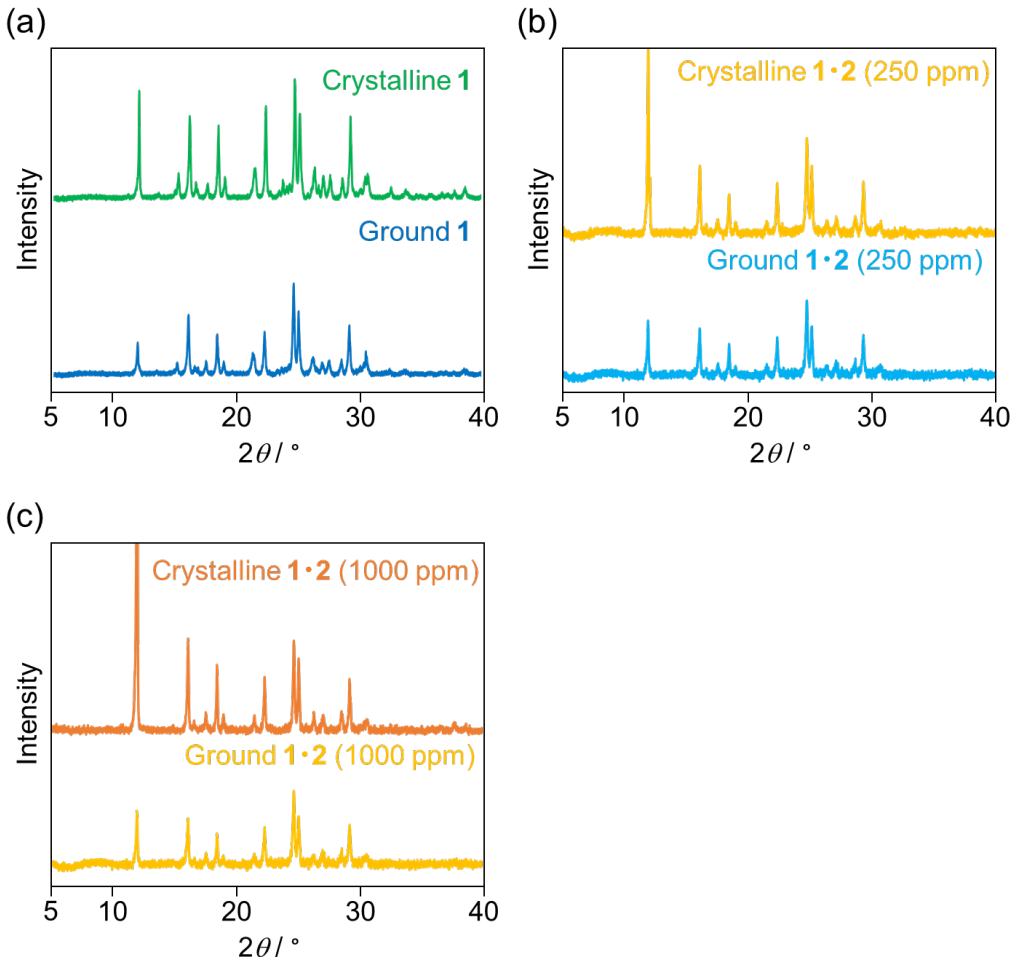

Fig. S6 PXRD patterns for emission switching of (a) **1**, (b) **1•2** (250 ppm), and (c) **1•2** (1000 ppm).

8. DSC thermograms

In the DSC diagrams, the only one endothermic peak corresponding to the melting point was observed for the crystalline and ground samples of **1** and **1•2** (Fig. S7)

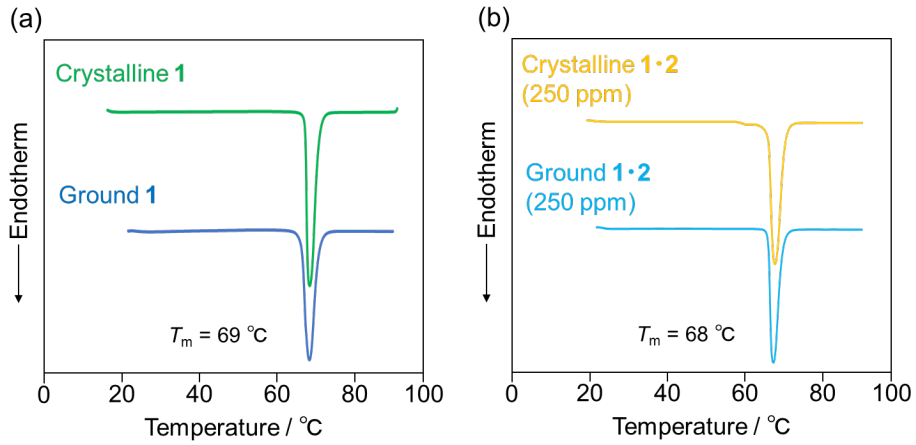

Fig. S7 DSC thermograms for the crystalline and ground samples of (a) **1** and (b) **1•2** (250 ppm).

9. Mechanoresponsive performance of doped crystals

Mechanoresponsive properties of doped crystals **1•2** were affected by the grinding pressure and crystal size (Fig. S8 and Table S2). The grinding pressure was recorded by using a digital force gauge. The emission intensity in the long-wavelength region was increased upon crushing crystalline **1•2** (250 ppm) into fine crystals with a relatively low pressure of 6–10 N cm^{-2}. Larger crystals tend to require a higher pressure to show comparable spectral changes relative to smaller crystals. Further strong grinding (40–70 N cm^{-2}) was required to sufficiently change the emission spectra.

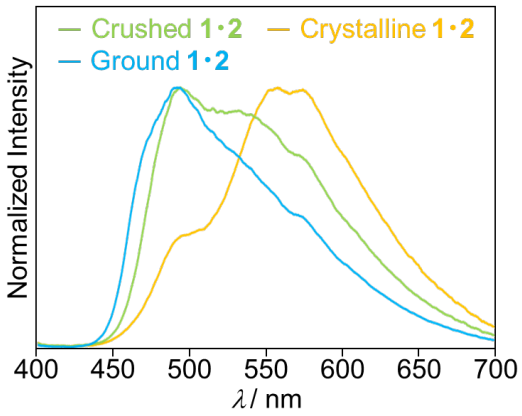

Fig. S8 Emission spectral change of doped crystal **1•2** (250 ppm) in response to crushing and griding (Entry 1 in Table S2, λ_{em} = 365 nm).

Table S2 The effect of crystal size of doped crystal **1•2** (250 ppm) on the crushing and grinding pressures.

Entry	Size (length×width×thickness) mm^3	Crushing pressure N cm^{-2}	Griding pressure N cm^{-2}
1	2.0×1.0×0.14	9.4	64
2	2.0×1.0×0.15	10.0	71
3	1.5×1.5×0.11	7.6	59
4	1.5×1.0×0.12	9.1	67
5	1.5×1.0×0.12	8.7	65
6	1.5×1.0×0.11	8.4	61
7	1.0×1.0×0.13	7.8	69
8	1.0×1.0×0.11	8.7	55
9	1.0×0.5×0.09	5.9	38
10	1.0×0.5×0.10	5.7	48

10. Measurements of fluorescence lifetimes

Spatially resolved fluorescence measurements were performed on a home-built wide-field/confocal microscope equipped with a Nikon Ti-E inverted fluorescence microscope. The fluorescence images were recorded using a color sCMOS camera (Dhyana 400DC, Tucsen Photonics). The 405-nm continuous wave laser (OBIS 405LX, Coherent) or 405-nm pulsed diode laser (PiL040X, Advanced Laser Diode System, 45-ps FWHM) was used to excite the samples. A dichroic mirror (Di02-R405, Semrock) and a longpass filter (ET425lp, Chroma) were used to filter the scattering from excitation light. To separate the fluorescence signals, bandpass filters (FF01-450/70, FF01-593/LP, Semrock) were used. An area of approximately 1 μm^2 on a target particle or region was spatially selected using a 100-μm pinhole to measure its spectrum and fluorescence lifetime. For the spectroscopy, only the emission that passed through the pinhole and a slit entered the imaging spectrograph (MS3504i, SOL instruments) equipped with a CCD camera (DU416A-LDC-DD, Andor). For time-resolved fluorescence measurements, the emitted photons were passed through the pinhole and then directed onto a single-photon avalanche diode (SPD-050, Micro Photon Devices). The signals from the detector were sent to a time-correlated single photon counting module (SPC-130EM, Becker & Hickl) for further analysis. The instrument response function of the system was about 100 ps. All the experiments were conducted at room temperature. The data were analyzed using ImageJ (http://rsb.info.nih.gov/ij/) and Origin 2021 (OriginLab).

Table S3 Fluorescence decay and rise times of crystalline and ground samples.

Sample	Region (nm)	$\tau_1{}^a$ (ns)	$\tau_2{}^a$ (ns)	$\tau_3{}^a$ (ns)	χ^2
Crystalline **1**	>425	7.2	–	–	1.4
Ground **1**	>425	6.9	–	–	1.8
Crystalline **1•2** (250 ppm)	415–485	2.0 (0.61)	3.7 (0.39)	–	1.2
	> 601	1.8 (–0.25)	7.3 (1.25)	–	1.1
	>425	0.8 (–0.02)	6.6 (1.02)	–	1.4
Crystalline **1•2** (1000 ppm)	415–485	1.0 (0.66)	2.8 (0.34)	–	0.70
	> 601	0.9 (–0.08)	7.7 (1.08)	–	1.1
	>425	0.6 (–0.009)	2.8 (0.326)	8.7 (0.683)	1.2
Ground **1•2** (250 ppm)	415–485	2.5 (0.23)	6.2 (0.77)	–	1.2
	> 601	2.1 (–0.18)	8.4 (1.18)	–	1.2
	>425	0.08 (–0.004)	2.8 (0.295)	7.1 (0.709)	1.2

[a] The fractional contribution f_n of the component is indicated in parentheses.

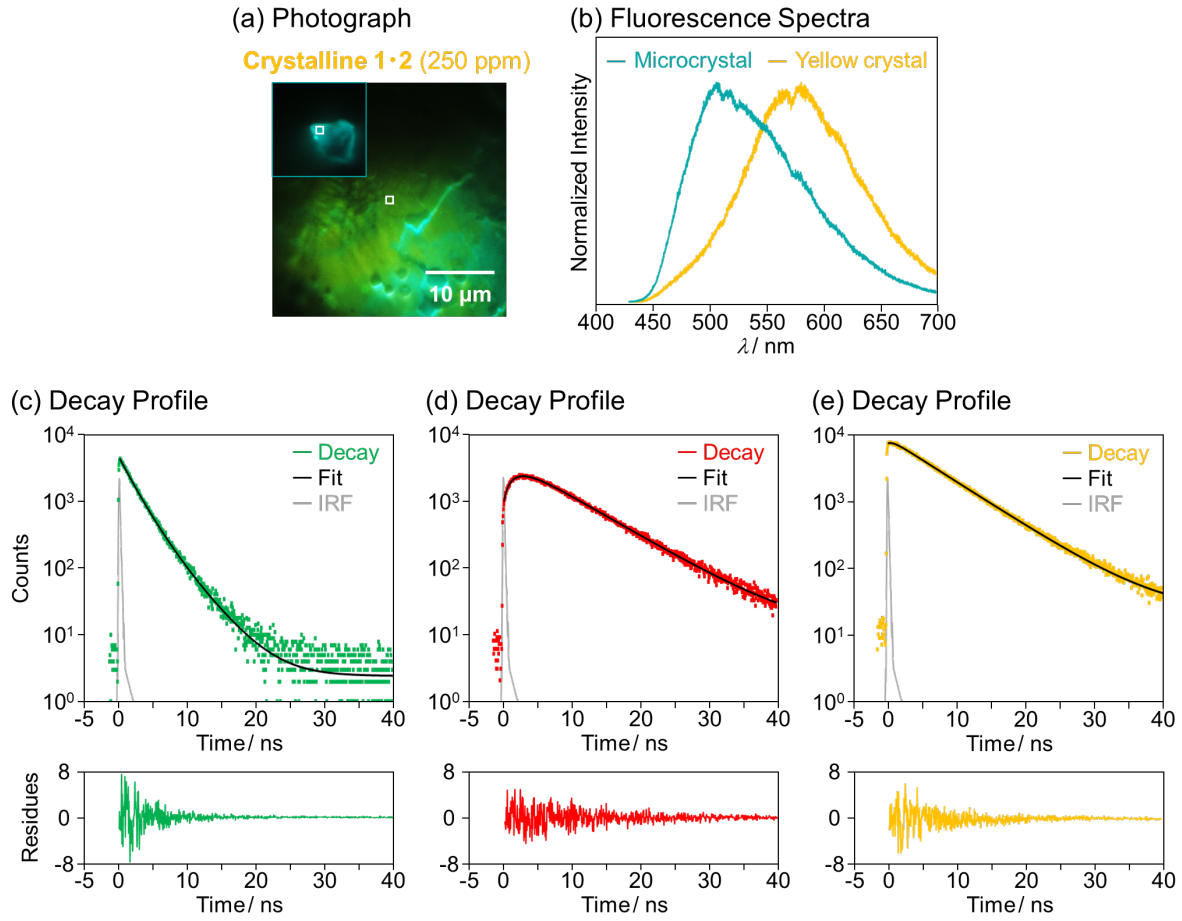

Fig. S9 Photographs, fluorescence spectra, and fluorescence decay profiles recorded by spatially resolved fluorescence microscopy (λ_{ex} = 405 nm). (a) Photographs of a yellow-emissive crystal and a blue-green-emissive microcrystal (inset) contained in crystalline **1•2** (250 ppm). The square marks indicate the measured locations of fluorescence spectra and fluorescence decay profiles. (b) Fluorescence spectra of blue-green-emissive microcrystal (blue-green line) and a yellow-emissive crystal (yellow line) contained in crystalline **1•2** (250 ppm). (c–e) Fluorescence decay profiles of a yellow-emissive crystalline **1•2** (250 ppm) monitored at 415–485 nm (green squares), >601 nm (red squares), and >425 nm (yellow squares). The black lines indicate multi-exponential curves fitted to the time profiles. The grey lines indicate the instrument response function (IRF).

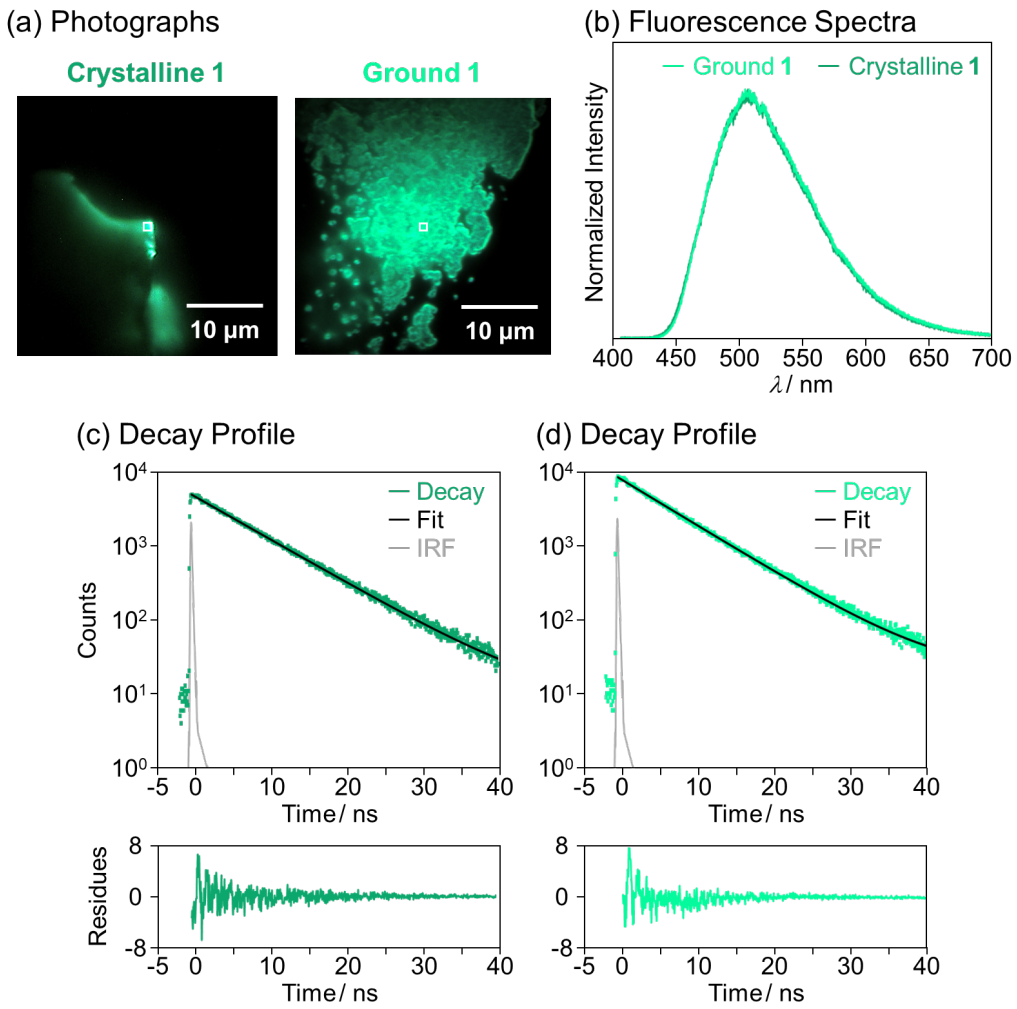

Fig. S10 Photographs, fluorescence spectra, and fluorescence decay profiles recorded by spatially resolved fluorescence microscopy (λ_{ex} = 405 nm). (a) Photographs of crystalline **1** and ground **1**. The square marks indicate the measured locations of fluorescence spectra and fluorescence decay profiles. (b) Fluorescence spectra of crystalline **1** (green line) and ground **1** (light-green line). (c and d) Fluorescence decay profiles of yellow-emissive crystalline **1** (green squares) and ground **1** (light-green squares) monitored at >425 nm. The black lines indicate multi-exponential curves fitted to the time profiles. The grey lines indicate the IRF.

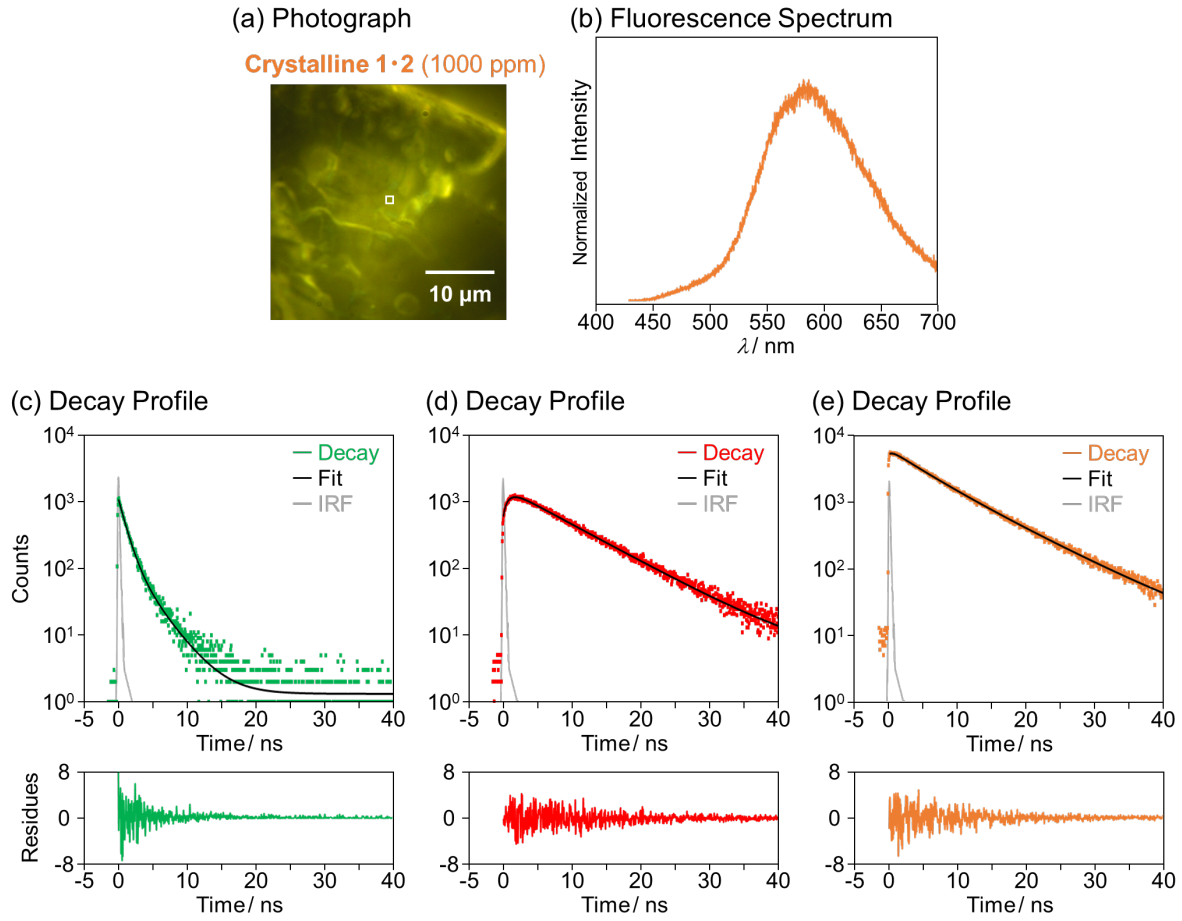

Fig. S11 Photograph, fluorescence spectrum, and fluorescence decay profiles recorded by spatially resolved fluorescence microscopy (λ_{ex} = 405 nm). (a) Photograph of crystalline **1•2** (1000 ppm). The square mark indicates the measured location of fluorescence spectrum and fluorescence decay profiles. (b) Fluorescence spectrum of crystalline **1•2** (1000 ppm). (c–e) Fluorescence decay profiles of crystalline **1•2** (1000 ppm) monitored at 415-485 nm (green squares), >601 nm (red squares), and >425 nm (orange squares). The black lines indicate multi-exponential curves fitted to the time profiles. The grey lines indicate the IRF.

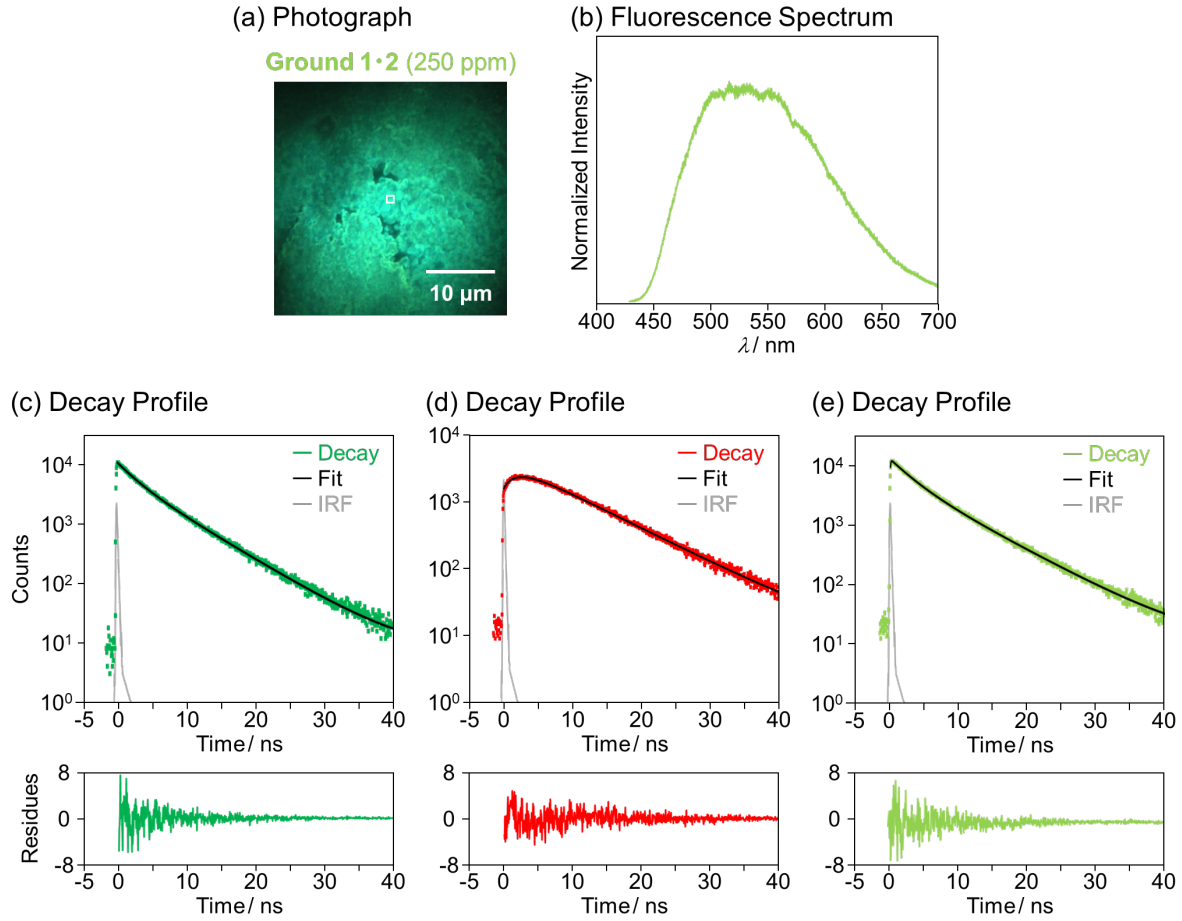

Fig. S12 Photograph, fluorescence spectrum, and fluorescence decay profiles recorded by spatially resolved fluorescence microscopy (λ_{ex} = 405 nm). (a) Photograph of ground **1•2** (250 ppm). The square mark indicates the measured location of fluorescence spectrum and fluorescence decay profiles. (b) Fluorescence spectrum of ground **1•2** (250 ppm). (c–e) Fluorescence decay profiles of ground **1•2** (250 ppm) monitored at 415–485 nm (green squares), >601 nm (red squares), and >425 nm (yellow-green squares). The black lines indicate multi-exponential curves fitted to the time profiles. The grey lines indicate the IRF.

11. References

1) R. Yoshida, T. Tachikawa, S. Ito, *Cryst. Growth. Des.*, 2022, **22**, 547.
2) M. Li, M. Zhao, S. Peng, *Inorg. Chem. Commun.*, 2013, **36**, 130.
3) Gaussian 16, Revision A.03, M. J. Frisch, G. W. Trucks, H. B. Schlegel, G. E. Scuseria, M. A. Robb, J. R. Cheeseman, G. Scalmani, V. Barone, G. A. Petersson, H. Nakatsuji, X. Li, M. Caricato, A. V. Marenich, J. Bloino, B. G. Janesko, R. Gomperts, B. Mennucci, H. P. Hratchian, J. V. Ortiz, A. F. Izmaylov, J. L. Sonnenberg, D. Williams-Young, F. Ding, F. Lipparini, F. Egidi, J. Goings, B. Peng, A. Petrone, T. Henderson, D. Ranasinghe, V. G. Zakrzewski, J. Gao, N. Rega, G. Zheng, W. Liang, M. Hada, M. Ehara, K. Toyota, R. Fukuda, J. Hasegawa, M. Ishida, T. Nakajima, Y. Honda, O. Kitao, H. Nakai, T. Vreven, K. Throssell, J. A. Montgomery, Jr., J. E. Peralta, F. Ogliaro, M. J. Bearpark, J. J. Heyd, E. N. Brothers, K. N. Kudin, V. N. Staroverov, T. A. Keith, R. Kobayashi, J. Normand, K. Raghavachari, A. P. Rendell, J. C. Burant, S. S. Iyengar, J. Tomasi, M. Cossi, J. M. Millam, M. Klene, C. Adamo, R. Cammi, J. W. Ochterski, R. L. Martin, K. Morokuma, O. Farkas, J. B. Foresman and D. J. Fox, Gaussian, Inc., Wallingford CT, 2016.
4) S. F. Boys and F. Bernardi, *Mol. Phys.*, 1970, **19**, 553.
5) K. Momma and F. Izumi, *J. Appl. Crystallogr.*, 2011, **44**, 1272.